Scripta Materialia 163 (2019) 77–81

Contents lists available at ScienceDirect

Scripta Materialia

journal homepage: www.elsevier.com/locate/scriptamat

Grain boundary wetting correlated to the grain boundary properties: A laboratory-based multimodal X-ray tomography investigation

J. Sun [a,b], Y. Zhang [b,*], A. Lyckegaard [a], F. Bachmann [a], E.M. Lauridsen [a], D. Juul Jensen [b]

[a] Xnovo Technology ApS, 4600 Køge, Denmark
[b] Department of Mechanical Engineering, Technical University of Denmark, 2800 Kgs. Lyngby, Denmark

ARTICLE INFO

Article history:
Received 2 December 2018
Received in revised form 3 January 2019
Accepted 5 January 2019
Available online xxxx

Keywords:
Grain boundary wetting
Grain boundary energy
Three-dimension tomography
X-ray diffraction
Laboratory diffraction contrast tomography

ABSTRACT

The penetration behavior of liquid gallium in aluminum is characterized using laboratory X-ray attenuation tomography and related to grain boundary properties obtained from the 3D grain map reconstructed by laboratory diffraction contrast tomography (LabDCT). The data is unique because more than 100 grain boundaries are analyzed. It is suggested that it is the grain boundary energy which determines if a boundary is wetted or not: low energy boundaries are much more resistant to liquid gallium than higher energy ones. The potentials of using laboratory diffraction contract tomography for statistical studies of grain boundaries are thereby demonstrated.
© 2019 Acta Materialia Inc. Published by Elsevier Ltd. All rights reserved.

Grain boundary wetting refers to the phenomenon that a liquid metal penetrates along the grain boundaries within polycrystalline solid metals. Replacement of the original grain boundary with the liquid layer generally causes intergranular brittle fracture in otherwise ductile metals and alloys. This is known as liquid metal embrittlement (LME), which can be a serious problem for certain materials processing scenarios such as welding and galvanizing as well as in nuclear reactors with a spallation target of liquid metal [1,2]. Among the many systems exhibiting LME (e.g. Al-Ga, Al-Hg, Zn-Ga and Cu-Bi), the Al-Ga system is the most widely studied, due to the low melting temperature of Ga (29.8 °C) and the fact that rapid penetration and subsequent replacement of grain boundaries in Al by liquid Ga occur both with and without an applied stress [3–5]. Furthermore, the Al boundaries with penetrated Ga can be imaged with scanning electron microscopy. It is known as gallium enhanced microscopy and has been used to characterize the microstructure of Al alloys [6,7].

The penetration of liquid Ga proceeds non-uniformly in the three-dimensional grain boundary network of Al. It is found to be related with the characters of the grain boundaries such as misorientation angle and Σ value of high angle boundaries [3,6,8–12]. This type of investigation requires characterization of both the Ga penetration path and the crystallographic characters of the grain boundaries. Table 1 summaries the characterization methods reported in previous studies. Early studies mainly employed bicrystals, which limits the statistics of the grain boundaries studied. X-ray computed tomography at synchrotron radiation facilities offers easy mapping of the 3D path that liquid Ga follows in polycrystalline samples. However, in these studies [3,9,10], characterization of the grain boundaries stills confines to known bicrystals or 2D examination of grain orientations on sectioned sample surfaces. A grain boundary is essentially a 3D structure and to fully describe it mesoscopically, five independent parameters are needed: three parameters for the misorientation between the two grains defining the grain boundary and two parameters for the inclination of the grain boundary plane [13]. With 2D characterization on sectioned sample surfaces, information on the grain boundary plane can only be obtained through stereological approaches with certain assumptions [14] and the method is therefore quite limited. With the development during the last two decades of novel X-ray based diffraction-imaging techniques, non-destructive 3D mapping of the grain structures including crystallography is now possible. The 3D X-ray crystallographic imaging by diffraction contrast tomography (DCT) originates from methods developed at high-energy synchrotron X-ray facilities [15–17]. This opened the possibility to study many aspects related to thermomechanical processing and damage mechanisms in polycrystalline materials. Examples of such studies include grain growth [18], grain rotation during sintering [19] and intergranular crack propagation during stress corrosion cracking [20]. The recently developed laboratory diffraction contrast tomography (LabDCT™), made the DCT technique available in the laboratory and thus enables a wider accessibility and routine use of the DCT technique for non-destructive, time-evolution experiments [21–23]. The DCT can be coupled with other 3D X-ray imaging approaches such as attenuation

* Corresponding author at: Technical University of Denmark, Produktionstorvet, Building 425, room 214, 2800 Kgs. Lyngby, Denmark.
E-mail address: yubz@mek.dtu.dk (Y. Zhang).

https://doi.org/10.1016/j.scriptamat.2019.01.007
1359-6462/© 2019 Acta Materialia Inc. Published by Elsevier Ltd. All rights reserved.

Table 1
Brief summary of previous experimental methods to study liquid metal embrittlement.

References	Methods to characterize Ga penetration	Methods to obtain grain orientation
[10]	Visual inspection	Bicrystals with known orientations
[8]	Transmission electron microscopy	• Bicrystals with known orientations • TEM Kikuchi diffraction patterns
[12]	Synchrotron X-ray tomography	Synchrotron X-ray diffraction
[9]	Synchrotron X-ray tomography	Bicrystals with known orientations
[3]	Synchrotron X-ray tomography	Electron backscattered diffraction
[6]	Scanning electron microscopy	Electron backscattered diffraction

contrast tomography (ACT) and phase contrast tomography, to characterize various other microstructural features.

In this work, characterization of the Ga penetration behavior in Al is correlated to a 3D characterization of the grain boundaries using a laboratory multimodal X-ray imaging approach. The polycrystalline microstructure, including both morphology and crystallographic orientation of the grains, is characterized by LabDCT. The misorientation and grain boundary plane normal are then extracted from the 3D grain map. The Ga penetration path is revealed by ACT and correlated with the grain boundaries.

The material used in this study is a fully recrystallized AA1050 aluminum alloy with mean grain size of 65 μm. A cylindrical sample with diameter of 1 mm was prepared using electrical discharge machining. LabDCT was conducted first, using the commercially available ZEISS Xradia 520 Versa X-ray Microscope equipped with the LabDCT module. Fig. 1(a) schematically illustrates the principles of LabDCT. The instrument uses a polychromatic, divergent X-ray beam. An aperture is placed between the source and the sample, to constrain the incoming X-ray beam. A beam-stop is placed between the sample and the detector blocking the transmitted X-rays and thereby increasing the sensitivity of the diffraction. A high-resolution detector is placed at the Laue focal plane with equal distance between source-sample and sample-detector. With this setup, the grains fulfilling the Bragg condition focus the divergent X-ray beams into a line in the diffraction pattern. Fig. 1(b) shows an example of such a diffraction pattern. The shadow of the beam-stop can be seen in the center. During acquisition, the sample is rotated 360° and a specified number of DCT scan projections are collected.

After the LabDCT scan, the top surface of the cylindrical sample is slightly scratched with a razor blade to break the oxidation layer. Liquid Ga is then placed in direct contact with the scratched sample surface and kept at 100 °C for 2 h in order for the Ga to penetrate and wet the grain boundaries. The Ga-treated sample is then scanned by ACT covering the approximately same sample volume as that already characterized by LabDCT. As the Ga is placed as a droplet on top of the sample, a gradient in the Ga concentration through the sample may exist. We however checked the Ga intensity averaged over all grain boundaries in the top and the bottom section of the investigated sample volume and found no significant difference between top and bottom.

The acquired diffraction contrast projections are reconstructed with GrainMapper3D™, developed by Xnovo Technology ApS. Both the crystallographic orientations and morphologies of more than 1000 grains are available from the reconstructed 3D grain map. With this information, the five parameters describing the misorientations across the grain boundaries and the grain boundary planes can be derived. Part of the reconstructed 3D grain map is shown in Fig. 2(a). The sample volume reconstructed from ACT visualizing the Ga wetted grain boundaries, cropped at approximately the same position, is shown in Fig. 2(b). The original reconstructed volume is further processed to enhance the visibility of Ga-wetted grain boundaries, which are seen brighter compared to the darker Al matrix in Fig. 2(b). It is clear that with the current treatment method the Ga fully penetrated the bulk of the sample. The penetration behavior of Ga into the Al grain boundaries is investigated by comparing slices clipped at the approximately same position in the sample volume. Fig. 2(c) and (d) reveals many grain boundaries visualized both by LabDCT and ACT, while there are also grain boundaries revealed by LabDCT that are not penetrated by Ga and hence not visible in the ACT. Moreover, the wetted grain boundaries are penetrated to different extents, with some grain boundaries appearing brighter than others. Five regions are highlighted as Regions 1 to 5 to exemplify the different responses of grain boundaries to liquid Ga penetration. The highlighted five regions in Fig. 2(d) are all surrounded by Ga wetted grain boundaries while each of the regions includes more than one grain, as revealed in the corresponding slice from LabDCT (Fig. 2(c)) where the grains within the individual regions are marked by numbers. The grain boundaries between these numbered grains in each region are not penetrated by Ga. These grain boundaries are termed 'unwetted' grain boundaries in the following text. The misorientation angles for the unwetted grain boundaries in the highlighted regions are calculated and listed in Table 2. All the unwetted grain boundaries in these regions, except the boundaries between grain 11 and 12, are low angle grain boundaries with misorientation angles lower than 10°.

Further investigation of the penetration behavior of the liquid Ga was done by exploring the intensity of Ga as a function of the misorientation angle for 115 grain boundaries. The maximum Ga intensity for each 3D grain boundary (measured based on all the ACT slices containing the grain boundary) is normalized to a value between 0 and 1 by dividing by the difference between the maximum and minimum Ga intensity in all measured grain boundaries. As shown in Fig. 3, in general, the normalized Ga intensity increases with increasing misorientation angle until a saturation plateau. It should be noted that the smallest misorientation angle shown in Fig. 3 is 0.3°, which demonstrates the fine angular resolution of LabDCT. The first important conclusion which can be drawn from Fig. 3 is that grain boundaries with identical misorientation angles can have very different Ga penetration behaviors.

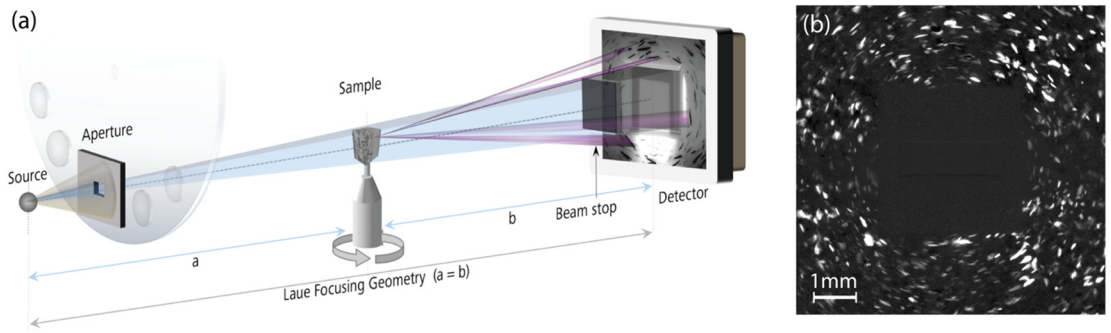

Fig. 1. Illustration of how LabDCT works. (a) Sketch showing the experimental setup of LabDCT in the laboratory X-ray microscope. (b) Example of a detector recording showing the diffraction signal from grains within the illuminated volume of the sample.

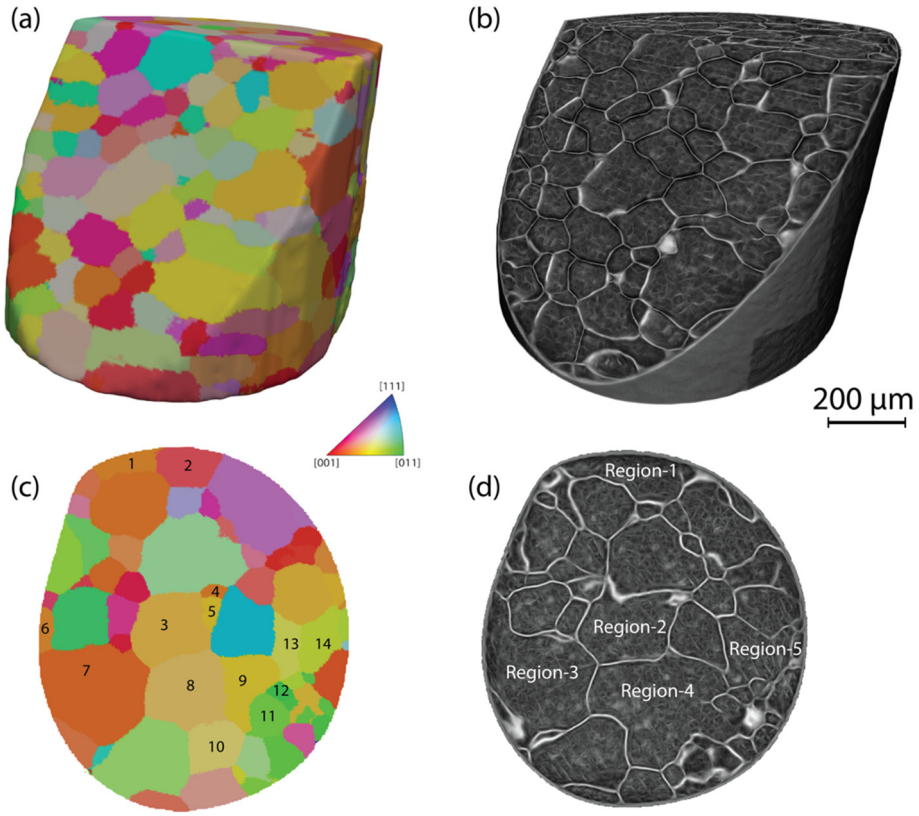

Fig. 2. Comparison of reconstructions from diffraction contrast and absorption contrast tomography. (a) 3D grain map reconstructed from laboratory diffraction contrast tomography, with coloring of the grains based on the rotation axis of the sample. (b) Reconstructed sample volume at a similar position in the sample as (a), determined by attenuation contrast tomography using edge enhancement: bright lines reveal the Ga-decorated grain boundaries. Comparison of the slices reconstructed from (c) laboratory diffraction contrast tomography and (d) attenuation contrast tomography. Regions 1–5 marked in (d) are regions with some of the grain boundaries not penetrated by Ga. The non-wetted grain boundaries are revealed from the diffraction contrast tomography in (c). Numbering of regions in (d) and grains in (c) correspond to Table 2.

Fig. 3 can be roughly be divided into three regions based on the Ga intensity: (i) unwetted grain boundaries (i.e. boundaries with a normalized intensity below 0.1) that are mostly low angle grain boundaries with misorientation angle smaller than 10°; (ii) wetted grain boundaries with high Ga intensity above 0.8 having misorientation angles larger than 15°; (iii) a 'transition' region with medium Ga intensity and misorientation angles in the range from 5 to 15°.

There are outliers to the categorized regions, and several of them are marked in Fig. 3. GB-1, GB-2 and GB-3 are high angle grain boundaries with medium Ga intensity. GB-4 is a high angle grain boundary that is unwetted. GB-5 belongs to region (ii): it has misorientation angle close to GB-3 and GB-4 but has a high Ga intensity. Further check of the misorientation angle and axis for the high angle grain boundaries with low to medium Ga intensity have shown that these outliers are CSL boundaries, judged according to the Brandon criterion [24]: GB-1 has misorientation of 21.2° around [−0.43, −0.63, −0.65], which is 3.7° deviated from the ideal Σ21a boundary and only slightly larger than the Brandon criterion (3.27°); GB-2 has misorientation of 36.8° around [−0.47, −0.64, −0.60], which is 4.5° deviated from the ideal Σ7 boundary and falls within the Brandon criterion (5.66°); GB-3 and GB-4 have misorientation of 57.3° around [0.55, 0.56, 0.62] and 59.9° around [−0.58, 0.58, 0.58], which are 4.0° and 0.1° deviated from the ideal Σ3 boundary, respectively and both are within the Brandon criterion (8.66°). GB-5 has misorientation of 59.2° around [0.37, 0.66, −0.65], which is a normal high angle grain boundary.

The inclination of grain boundary plane for GB-3 and GB-4 is analyzed to investigate the possible reasons for different Ga penetration behaviors given that both boundaries are Σ3 boundaries. Fig. 4(a) and (b) shows 3D volume rendering of GB-3 and GB-4 respectively, with the two grains forming the grain boundary. The distribution of grain boundary plane normal is calculated and shown in standard stereographic projections in Fig. 4(c) and (d) (meshing grain boundaries and determining grain boundary normals using Dream3D® [25]). It can be seen that the grain boundary plane normal distribution for GB-4 has the peak much closer to the {111} pole compared with GB-3.

From the current experimental evidences, it is suggested that the variations in Ga wetting behaviors are closely related to the energies of grain boundaries: (i) most of the unwetted boundaries are low angle boundaries (see Fig. 3) and for this category it is generally assumed that the boundary energy increases with increasing misorientation angle according to the Read-Shockley equation [27] and this matches well with the fact that the Ga intensity increases with increasing misorientation angle in the range from 5 to 12°; (ii) the 'outlier' high angle grain boundaries that have low or medium Ga intensity are found to be CSL boundaries with low Σ values, which are known to have lower energies; (iii) previous MD simulation results have shown that for Σ3

Table 2
The misorientation angle of the unwetted grain boundaries marked by numbers in Fig. 2(c,d).

Regions in Fig. 2(d)	Region 1	Region 2	Region 3	Region 4	Region 4	Region 4	Region 5
Neighboring grains	1&2	3&5	6&7	8&10	8&9	11&12	13&14
Misorientation (°)	7.7	8.1	4.9	5.7	4.2	59.9	3.0

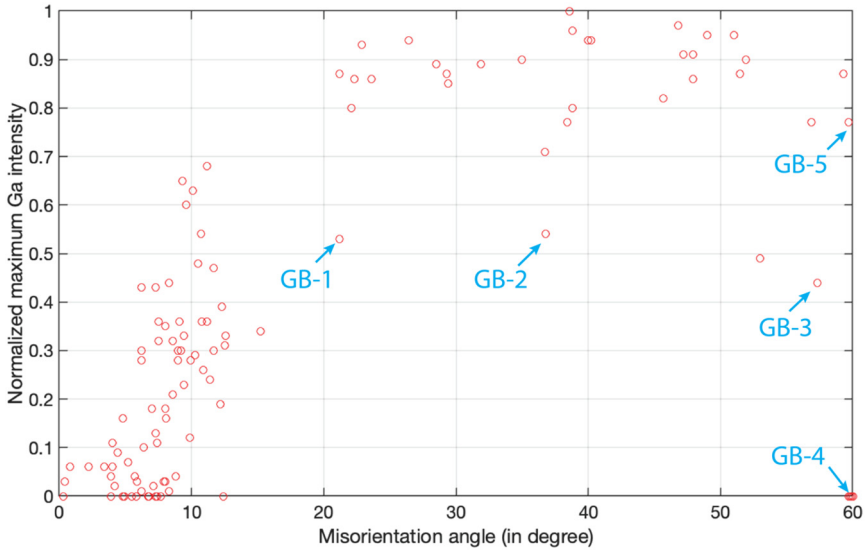

Fig. 3. Normalized maximum intensity of Ga plotted as a function of misorientation angle of the grain boundaries. Five grain boundaries (GB-1, GB-2, GB-3, GB-4 and GB-5) are highlighted as examples for further discussion.

boundaries, boundaries with planes closer to {111} have lower energy [28–30], and thus that GB-4 should have lower energy compared to GB-3, which matches the lower Ga intensity. It is known that the grain boundary energy is not determined only by the five parameters characterized here – also the atomic structural arrangement across the boundary may be of importance. An investigation of such atomic arrangement is however not possible with the present experimental method and is thus outside the scope of this work.

The present work has documented the potentials of laboratory multimodal X-ray tomography for characterization of sample volumes large enough for statistical studies of correlations between the metal microstructure and grain boundary wetting. For the present Al-Ga system, the grain boundary plane and misorientation has been correlated to the Ga wetting for 115 boundaries and it is suggested that it is the grain boundary energy which determines the preferential Ga penetration path in Al matrix.

The experimental approach presented in this paper provides a complete 3D description of the grain boundary network which can be used as input for and validation of grain boundary models. Advantages of this experimental method include: (i) both the grain boundary plane normal and the misorientation angles can readily be obtained, (ii) a large number of boundaries can be characterized relatively quickly, (iii) the method operates in the laboratory so no beamtime at synchrotron facilities is required and (iv) the method is non-destructive allowing subsequent processing and thus enabling studies of the microstructural evolution.

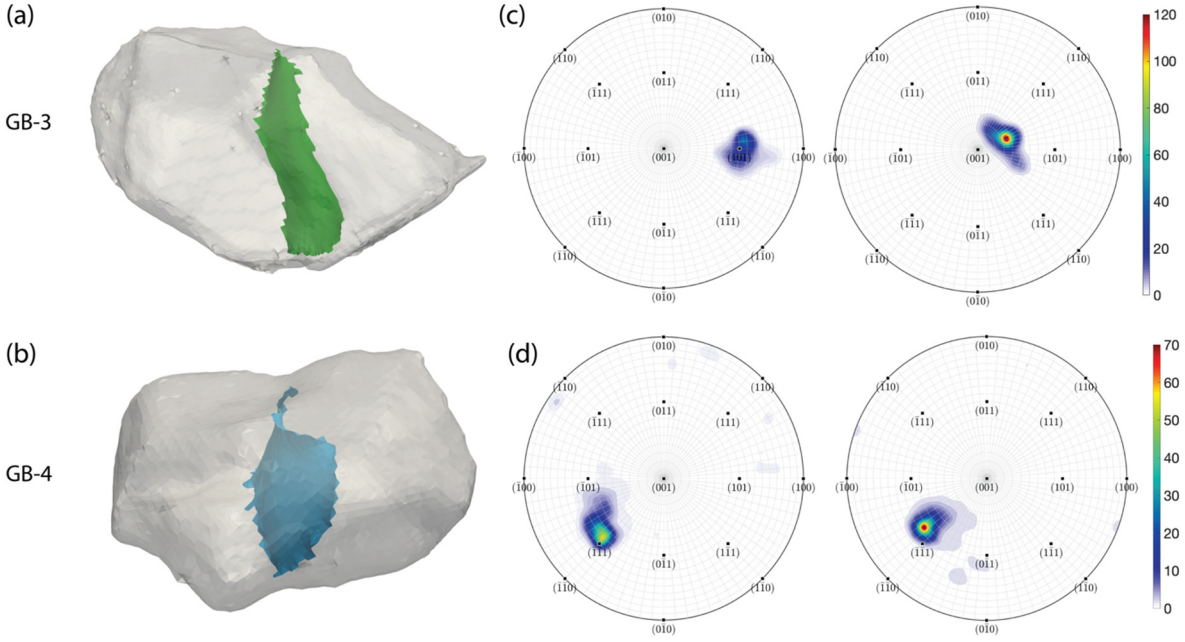

Fig. 4. Volume rendering and plane normal distribution of the grain boundaries highlighted in Fig. 3. (a) and (b) are volume rendering of GB-3 and GB-4 respectively, with the two grains forming the grain boundary. (c) and (d) are standard projections showing the distributions of grain boundary normal in the crystal system of the two grains forming the boundary, plotted using a software package, MTEX [26].

Acknowledgement

This work is partially funded by the Innovation Fund Denmark (IFD) under the project 'Multimodal 4D Characterization of Materials in the Laboratory' (case number: 5190-00044B) and has furthermore received funding from the European Research Council (ERC) under the European Union's Horizon 2020 research and innovation programme (grant agreement No 788567).

References

[1] M.G. Nicholas, C.F. Old, J. Mater. Sci. (1979) 1–18.
[2] H.S. Nam, D.J. Srolovitz, Acta Mater. 57 (2009) 1546–1553.
[3] M. Kobayashi, H. Toda, K. Uesugi, T. Ohgaki, T. Kobayashi, Y. Takayama, B.G. Ahn, Philos. Mag. 86 (2006) 4351–4366.
[4] T. Ohgaki, H. Toda, I. Sinclair, J.Y. Buffire, W. Ludwig, T. Kobayashi, M. Niinomi, T. Akahori, Mater. Sci. Eng. A 427 (2006) 1–6.
[5] R.C. Hugo, R.G. Hoagland, Scr. Mater. 38 (1998) 523–529.
[6] J. Hagström, O.V. Mishin, B. Hutchinson, Scr. Mater. 49 (2003) 1035–1040.
[7] O.V. Mishin, L. Östensson, A. Godfrey, Metall. Mater. Trans. A 37 (2006) 489–496.
[8] R.C. Hugo, R.G. Hoagland, Acta Mater. 27 (2000) 423–430.
[9] W. Ludwig, E. Pereiro-López, D. Bellet, Acta Mater. 53 (2005) 151–162.
[10] J.A. Kargol, D.L. Albright, Metall. Trans. A. 8 (1977) 27–34.
[11] H.S. Nam, D.J. Srolovitz, Phys. Rev. Lett. 99 (2007) 751–754.
[12] W. Ludwig, S.F. Nielsen, H.F. Poulsen, D. Bellet, Defect and Diffusion Forum, 194-199, 2001 1319–1330.
[13] G.S. Rohrer, D.M. Saylor, B. El Dasher, B.L. Adams, A.D. Rollett, P. Wynblatt, Z. Metallkd. 95 (2004) 197–214.
[14] D.M. Saylor, B.S. El Dasher, A.D. Rollett, G.S. Rohrer, Acta Mater. 52 (2004) 3649–3655.
[15] W. Ludwig, P. Reischig, A. King, M. Herbig, E.M. Lauridsen, G. Johnson, T.J. Marrow, J.Y. Buffière, Rev. Sci. Instrum. 80 (2009) 033905–033909.
[16] W. Ludwig, S. Schmidt, E.M. Lauridsen, H.F. Poulsen, J. Appl. Crystallogr. 41 (2008) 302–309.
[17] G. Johnson, A. King, M.G. Honnicke, J. Marrow, W. Ludwig, J. Appl. Crystallogr. 41 (2008) 310–318.
[18] J. Zhang, Y. Zhang, W. Ludwig, D. Rowenhorst, P.W. Voorhees, H.F. Poulsen, Acta Mater. 156 (2018) 76–85.
[19] J.M. Dake, J. Oddershede, H.O. Sørensen, T. Werz, J.C. Shatto, K. Uesugi, S. Schmidt, C.E. Krill III, Proc. Natl. Acad. Sci. U. S. A. 113 (2016) E5998–E6006.
[20] M. Herbig, A. King, P. Reischig, H. Proudhon, E.M. Lauridsen, J. Marrow, J.Y. Buffière, W. Ludwig, Acta Mater. 59 (2011) 590–601.
[21] C. Holzner, L. Lavery, H. Bale, A. Merkle, S. McDonald, P. Withers, Y. Zhang, D. Juul Jensen, M. Kimura, A. Lyckegaard, P. Reischig, E.M. Lauridsen, Micros. Today 24 (2016) 34–43.
[22] S.A. McDonald, P. Reischig, C. Holzner, E.M. Lauridsen, P.J. Withers, A.P. Merkle, M. Feser, Nat. Sci. Rep. 5 (2015) 14665.
[23] J. Sun, A. Lyckegaard, Y. Zhang, S.A. Catherine, B.R. Patterson, F. Bachmann, N. Gueninchault, H. Bale, C. Holzner, E. Lauridsen, D. Juul Jensen, IOP Conf. Ser.: Mater. Sci. Eng. 219 (2017), 012039–6. .
[24] D.G. Brandon, Acta Metall. Mater. 11 (1966) 1479–1484.
[25] M.A. Groeber, M.A. Jackson, Integr. Mater. 3 (2014) 3009–3017.
[26] F. Bachmann, R. Hielscher, H. Schaeben, Solid State Phenom. 160 (2010) 63–68.
[27] W.T. Read, W. Shockley, Phys. Rev. 78 (1950) 275–289.
[28] D.L. Olmsted, Acta Mater. 57 (2009) 2793–2799.
[29] D.L. Olmsted, S.M. Foiles, E.A. Holm, Acta Mater. 57 (2009) 3694–3703.
[30] K. Głowiński, PhD thesis, 2015.